BNL-224704-2023-JAAM

Record quantum efficiency from strain compensated superlattice GaAs/GaAsP photocathode for spin polarized electron source

J. Biswas, L. Cultrera

To be published in "AIP Advances"

August 2023

Instrumentation Division

Brookhaven National Laboratory

U.S. Department of Energy

USDOE Office of Science (SC), Basic Energy Sciences (BES) (SC-22)

Notice: This manuscript has been authored by employees of Brookhaven Science Associates, LLC under Contract No.DE-SC0012704 with the U.S. Department of Energy. The publisher by accepting the manuscript for publication acknowledges that the United States Government retains a non-exclusive, paid-up, irrevocable, world-wide license to publish or reproduce the published form of this manuscript, or allow others to do so, for United States Government purposes.

DISCLAIMER

This report was prepared as an account of work sponsored by an agency of the United States Government. Neither the United States Government nor any agency thereof, nor any of their employees, nor any of their contractors, subcontractors, or their employees, makes any warranty, express or implied, or assumes any legal liability or responsibility for the accuracy, completeness, or any third party's use or the results of such use of any information, apparatus, product, or process disclosed, or represents that its use would not infringe privately owned rights. Reference herein to any specific commercial product, process, or service by trade name, trademark, manufacturer, or otherwise, does not necessarily constitute or imply its endorsement, recommendation, or favoring by the United States Government or any agency thereof or its contractors or subcontractors. The views and opinions of authors expressed herein do not necessarily state or reflect those of the United States Government or any agency thereof.

Record quantum efficiency from strain compensated superlattice GaAs/GaAsP photocathode for spin polarized electron source

Jyoti Biswas,[1] Luca Cultrera,[1, a)] Wei Liu,[1] Erdong Wang,[1] John Skaritka,[1] Kim Kisslinger,[1] S.D. Hawkins,[2] S.R. Lee,[2] and J.F. Klem[2]
[1)]*Brookhaven National Laboratory, Upton, New York 11973, USA*
[2)]*Sandia National Laboratories, Albuquerque, New Mexico 87185, USA*

(Dated: 16 July 2023)

Photocathodes based on GaAs and other III-V semiconductors are capable of producing highly spin-polarized electron beams. GaAs/GaAsP superlattice photocathodes exhibit high spin polarization; however, the quantum efficiency (QE) is limited to 1% or less. To increase the QE, we fabricated a GaAs/GaAsP superlattice photocathode with a Distributed Bragg Reflector (DBR) underneath. This configuration creates a Fabry-Perot cavity between the DBR and GaAs surface, which enhances the absorption of incident light and, consequently, the QE. These photocathode structures were grown using molecular beam epitaxy and achieved record quantum efficiencies exceeding 15% and electron spin polarization of about 75% when illuminated with near-bandgap photon energies.

I. INTRODUCTION

Polarized electron sources play a crucial role in various fields of fundamental research, including condensed matter physics and elementary particle physics. Polarized electron sources are employed in polarized electron microscopy[1] to study domain walls in ferromagnetic materials. Polarized positron beams can be generated from polarized electron beams by impinging on high Z-target material[2]. Notably, the International Linear Collider, which is currently under development, is designed to facilitate the collision of spin-polarized electrons and positrons at high energies in the TeV range. The Electron Ion Collider[3] that will be operated in the USA also requires a spin-polarized electron source for nuclear physics study. Most facilities require a few hundred microamperes of current that can be easily produced by the current state-of-the-art electron sources[4]. Other facilities such as the Large Hadron electron Collider plan to operate at a high average current of 20 mA[5], which is beyond the current state of the art.

Currently, spin-polarized electron sources rely on the utilization of GaAs-based photocathodes. The activation of GaAs involves the deposition of a small amount of cesium and an oxidant, typically oxygen or NF3, onto the surface[6,7]. This process creates negative electron affinity[8,9], a condition in which the vacuum level lies below the conduction band minimum in the bulk. When the NEA condition is achieved electron at the bottom of the conduction band can still escape into the vacuum thus photoemission increases. Bulk GaAs with traditional Cs-O activation provides a high Quantum Efficiency (QE) of around 10%, however, the maximum polarization is limited to 50% due to the degeneracy of the heavy-hole and light-hole at the $2p_{3/2}$ band state. Growing the GaAs photocathode strained eliminates the degeneracy thus spin polarized electrons can be extracted from one of the bands.

In the 1990s strained GaAs grown on GaAsP showed improved electron spin polarization (ESP) of 75-80%, whereas QE was limited to only about 0.3%[10]. Through the use of strained superlattices (SL) based on GaAs/GaAsP, it was possible to leverage quantum well structures to increase the separation between heavy and light hole bands and achieve even higher spin polarization (up to 85%) and QE (just above 1%)[11]. A higher number of SL pairs increases the QE, however, it contributes to strain relaxation and thus reduction of electron spin polarization. To increase the QE, the strain-compensated GaAs/GaAsP SL was proposed, which employed opposing strain in alternating layers to avoid critical thickness limitations. The strain compensated SL reduced the defect density, yielding a maximum QE of 1.6% and electron spin polarization of 92%[12]. Similar spin polarization is reported in many facilities, however, the QE lies around 1% or lower at near band gap photon energies[11,13,14].

II. CATHODE WITH DISTRIBUTED BRAGG REFLECTOR

A polarized electron beam with a high average current requires high power laser, which can adversely increase the temperature of the cathode and contribute the cathode QE degradation[15]. Photocathodes with high QE can lower the laser power requirement and thus reduce the laser-induced cathode heating and QE degradation. A distributed Bragg reflector (DBR) grown underneath the SL with a buffer medium layer creates a Fabry Perot resonator that effectively traps the light and enhances the QE[16,17]. Instead of laser light passing through the cathode, it reflects repeatedly within the cavity, increasing photon absorption, which in turn, improves the QE. Photocathodes with DBR structure were first reported in 1993[18] and studied in subsequent years[19,20]. Such a structure demonstrated record performance in achieving ESP of 84% and QE of 6.4% at 776 nm laser wavelength[16]. As the number of layers increases the growth of such structure with both high QE and ESP becomes increasingly challenging.

The structural element of the photocathode used in this work is illustrated in Fig. 1. The DBR consists of alternating layers of high (n_H) and low (n_L) index of refraction material. The high refractive index layer is $GaAs_{0.81}P_{0.19}$ and low refractive index layer is $AlAs_{0.78}P_{0.22}$. For a high reflectivity at a certain wavelength λ_B, the thickness of the DBR layers are, $\lambda_B/4n_H$, and $\lambda_B/4n_L$ respectively[18]. The bandwidth over which the DBR has high reflectivity can be expressed as[18],

$$\Delta\lambda_B = \frac{4\lambda_B}{\pi} sin^{-1}\left(\frac{n_H - n_L}{n_H + n_L}\right) \quad (1)$$

[a)]Electronic mail: lcultrera@bnl.gov

GaAs	5 nm	p = 5x10^{19} cm^{-3}	
$GaAs_{0.62}P_{0.38}$	4 nm	p = 5x10^{17} cm^{-3}	30 pairs
GaAs	4 nm	p = 5x10^{17} cm^{-3}	
$GaAs_{0.81}P_{0.19}$	300 nm	p = 5x10^{18} cm^{-3}	
$AlAs_{0.78}P_{0.22}$	65 nm	p = 5x10^{18} cm^{-3}	10 pairs
$GaAs_{0.81}P_{0.19}$	55 nm	p = 5x10^{18} cm^{-3}	
$GaAs_{0.81}P_{0.19}$	2000 nm	p = 5x10^{18} cm^{-3}	
GaAs->$GaAs_{0.81}P_{0.19}$	2750 nm	p = 5x10^{18} cm^{-3}	
GaAs buffer	200 nm	p = 5x10^{18} cm^{-3}	
GaAs substrate		p > 1x10^{18} cm^{-3}	

FIG. 1. Schematic of the superlattice GaAs photocathode with DBR structure. The GaAs surface layer was capped with amorphous As after the epitaxial growth.

The DBR layer consists of 10 pairs of $GaAs_{0.81}P_{0.19}$ and $AlAs_{0.78}P_{0.22}$. The index of refraction and absorption coefficient of $GaAs_{0.81}P_{0.19}$ have been estimated considering the band edge shift due to the change in composition using available data[21]. The index of refraction of AlP and AlAs were used to perform a linear interpolation as a function of the P content to obtain the index of refraction of $AlAs_{0.78}P_{0.22}$ in the spectral region between 600 and 840 nm[22,23]. The refractive index are estimated as $n_H = 3.554$, and $n_L = 2.992$ respectively and thickness are around $d_H = 65nm$ and $d_L = 55nm$ respectively. Bandwidth $\Delta\lambda_B$ estimated around 85 nm with λ_B equal 780 nm, the drive laser wavelength. The Fabry-Perot resonating cavity has a round trip time estimated to be no larger than about 40 fs. On the other hand, the round trip losses, dominated by the transmission losses at the interface with the vacuum, are close to 75%, yielding a Q-factor of the Fabry-Perot at 780 nm of about 130. Given the large round trip losses and the fact that photon absorption is still taking place only in the superlattice, we do not expect the increase in the response time to be larger than a few hundred femtoseconds.

The samples were grown in a molecular beam epitaxy (MBE) system at Sandia National Laboratories. Samples were grown on a p-type (>$1 \times 10^{18}/cm^3$) (100) GaAs wafer (lattice constant 5.653 Angstrom), 200 nm buffer layer of p-type (>$5 \times 10^{18}/cm^3$) GaAs (0.0% lattice strain) was used to regrow the GaAs surface and provide a flat surface. Over the GaAs buffer, a graded composition layer from GaAs to $GaAs_{0.81}P_{0.19}$ with a thickness of about 2750 nm with p-type doping (>$5 \times 10^{18}/cm^3$) was used to slowly decrease the lattice constant of the surface to 5.614 Angstrom. Around 200 nm of $GaAs_{0.81}P_{0.19}$ was grown on top of that as a base layer for the DBR structure. The DBR consists of $AlAs_{0.78}P_{0.22}$ and $GaAs_{0.81}P_{0.19}$ layers with a thickness of 65 and 55 nm respectively. A 300 nm base layer will be used to provide the strain compensating lattice constant for the growth of the SL and the optical thickness for the tuning of the Fabry-Perot resonator. The strain compensated (-0.7%/+0.7%) SL structure consists of 30 pairs of p-type ($5 \times 10^{17}/cm^3$) $GaAs_{0.62}P_{0.38}/GaAs$ (4/4 nm thickness). The structure is terminated with a 5 nm highly p-doped (carbon doping of $5 \times 10^{19}/cm^3$) GaAs.

Fig. 2 shows measured photoluminescence and reflectance of the SL-DBR. During photoluminescence measurement a non polarized frequency doubled Nd:YAG laser at 532 nm was used as excitation source. The SL-DBR structure photoluminescence peaks around 782 nm, and minimum reflectance is observed at around 781 nm. This is close to our design requirements, since 780 nm is typically the drive laser wavelength. The simulated DBR with 10 pairs shows high reflectance (above 95% at 780 nm) and wide bandwidth $\Delta\lambda_B$.

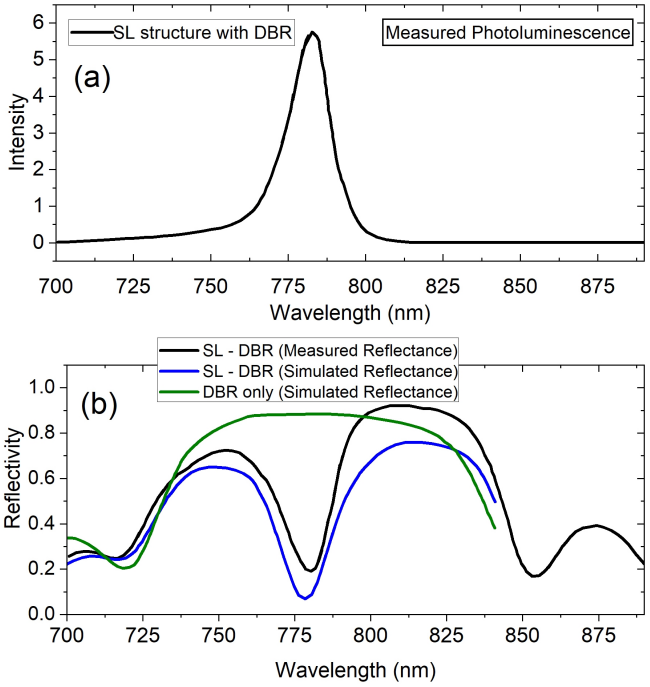

FIG. 2. (a) Measured photoluminescence of SL structure with DBR, (b) measured and simulated reflectance of SL-DBR, and simulated reflectance of DBR.

We evaluated the crystal quality of the SL-DBR photocathode using transmission electron microscopy (TEM) at Center for Functional Nanomaterials (CFN) at Brookhaven National Laboratory. TEM lamella were made using the in-situ lift-out method with a FEI Helios G5 UX DualBeam FIB/SEM with final Ga+ milling performed at 2 keV. TEM analysis was performed with a FEI Talos F200X TEM/STEM at an operating voltage of 200 keV with EDS data collected by 4 in-column integrated SSD Super-X detectors. Fig. 3 shows cross-sectional TEM/STEM images and EDS map of the SL-DBR photocathode. We did not observe any stacking faults or misfit dislocations[24] in the SL structure. Some threading dislocations are observed in the DBR structure.

III. QE AND SPIN POLARIZATION

Photocathode samples were evaluated within a low-voltage retarding-field Mott polarimeter located at Brookhaven National Laboratory (BNL). A picture of this Mott polarimeter system is shown in Fig. 4. A new sample was attached to the cathode puck and loaded into the chamber through the load-lock manipulator that was baked at 200°C for 72 hours. The 3" GaAs wafer was cleaved in 4 identical quarters and the data reported in Fig. 2, Fig. 4, and Fig. 5 were obtained using

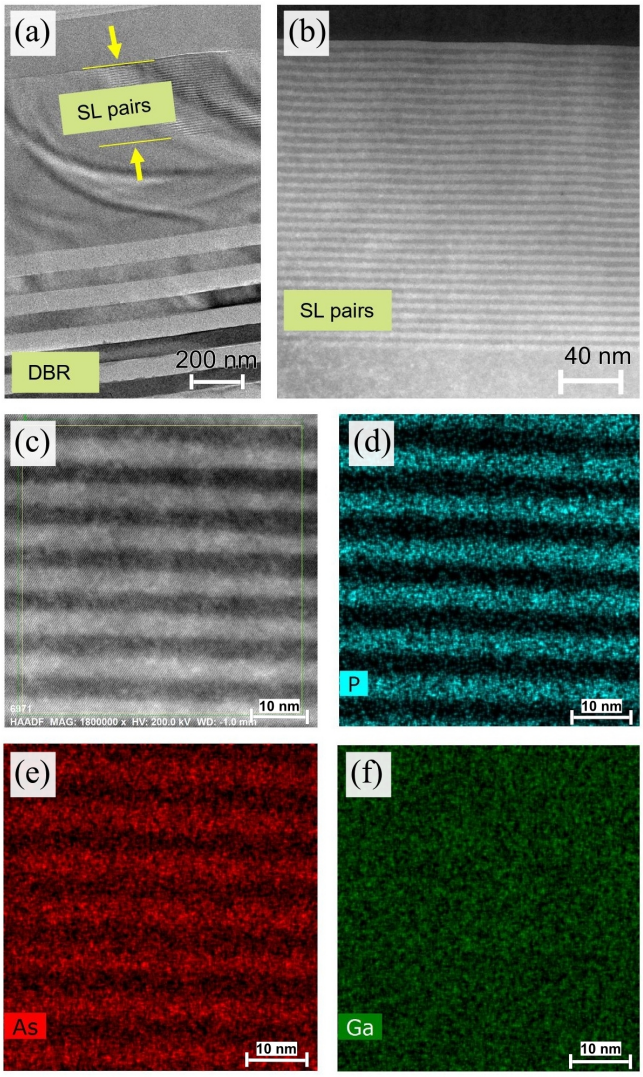

FIG. 3. (a) Cross-sectional TEM images of SL-DBR GaAs showing both SL and DBR pairs. Bend contours are visible which are associated with the bent sample with respect to the incident electron beam. The number of DBR-pairs was 10. (b) STEM image showing uniform SL-pairs (c) STEM image of a few SL-pairs, (d) EDS map of P, (e) EDS map of As, and (f) EDS map of Ga.

specimens obtained from samples obtained from wafer area close to the center. The sample was then heated to 500°C for 2 hours to remove the As cap and contamination from the surface under the vacuum pressure of 10^{-11} Torr scale. Then, the sample was activated at room temperature to form a negative electron affinity (NEA) surface using the alternate deposition of Cs and O_2 commonly known as "yo-yo activation"[8,25]. The QE of the sample was scanned with a laser with a wavelength ranging from 700 nm to 800 nm. A circularly polarized laser generated by a linear film polarizer and a quarter-wave plate finally illuminated the sample to obtain spin-polarized electrons, which were transferred into the spin detector through the spin deflector and transfer lens to measure the electron spin polarization (ESP). Laser spot size during the QE and ESP measurement was around 2 mm^2.

The measured QE and ESP for the photocathode sample (near the center of the wafer) as a function of wavelength are shown in Fig. 5. We performed the measurement both near

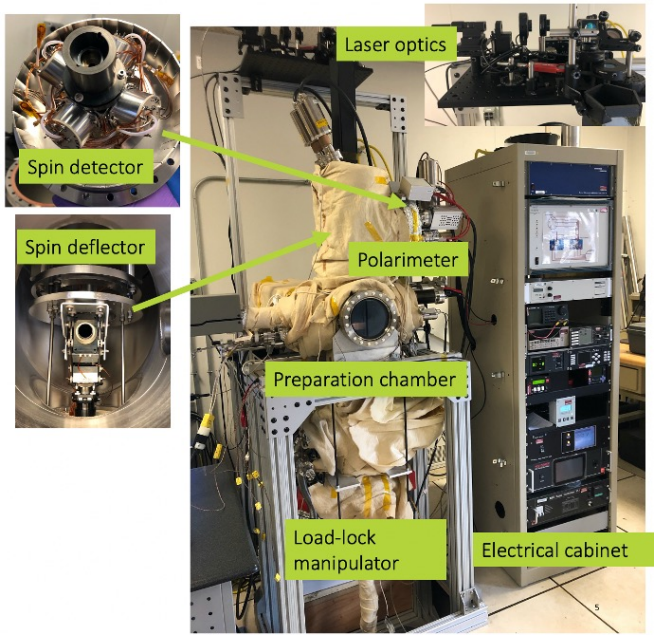

FIG. 4. The picture of the Mott polarimeter system at BNL, which is used for activation of photocathode and measurement of the QE and ESP.

the center and close the edge of a 3-inch wafer. The peak QE obtained near the center exceeds 15%, which is the highest ever reported photocathode QE at near-bandgap photon energies for SL-based photocathodes. The maximum ESP found near the center of the wafer is close to 70%. Close to the edge of the wafer, the maximum QE is just above 10% and ESP is above 75% (Fig. S1 in supplementary material). Near the center of the wafer, both ESP and QE are close to the design requirements- both QE and ESP maximize at around 780 nm. However, away from the center peak QE position deviates from the design requirements. Given the uniform in plane biaxially strain applied to the grown structure we do not expect index of refraction anisotropy to have developed similarly to other previously reported structures[16].

A possible explanation for the non-uniformity across the 3-inch wafer may be related to a non-uniform temperature across the wafer during the growth process leading to deviations from ideal composition and thickness. Our reflectance measurement showed that reflectance peaks vary from location to location, and at the center of the wafer it peaks around 780 nm wavelength. Fig. 6 shows the reflectance of the wafer at different locations, marked by A, B, C, D, and E. Position C is close to the center of the 3-inch wafer, and position E is near the edge of the wafer. We are currently exploring different experimental conditions aimed at increasing the temperature uniformity to verify this hypothesis and meet design parameters over larger areas of the wafer.

Though we obtained a very high QE at around 776 nm laser illumination, the peak ESP was still lower than the target ESP of 85%. We are currently optimizing the SL-pair design to achieve higher ESP.

In table I, we compared our results with different polarized photocathodes previously reported using the figure of merit (P^2QE). Our photocathode exhibits higher values for the figure of merit compared to the previously reported values when

operated at a wavelength of 776 nm.

TABLE I. Figure of merit for for different polarized electron sources.

Cathode	Reference	P%	QE%	P^2QE%
GaAs – $GaAsP_{0.36}$	SLAC/SVT[26]	86	1.2	0.89
GaAs – $GaAsP_{0.38}$	Nagoya[12]	92	1.6	1.35
GaAs – $GaAsP_{0.35}$ (DBR)	JLAB/SVT[16]	84	6.4	4.52
GaAs – $GaAsP_{0.38}$ (DBR)	SNL/BNL	62	15.5	5.96

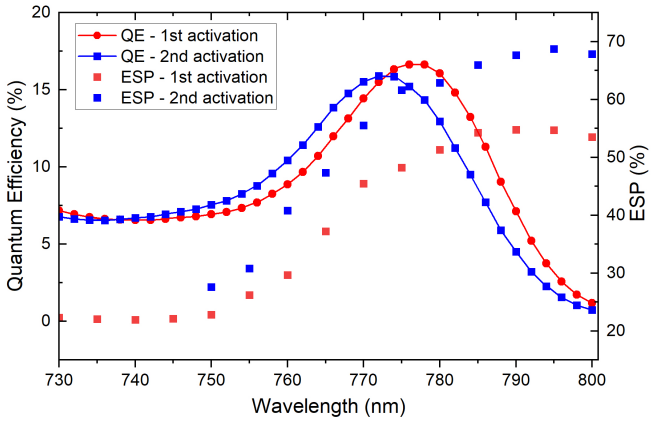

FIG. 5. The QE and electron-spin polarization for the GaAs/GaAsP superlattice DBR photocathode as a function of the wavelength, measured at two different location near the center of the wafer.

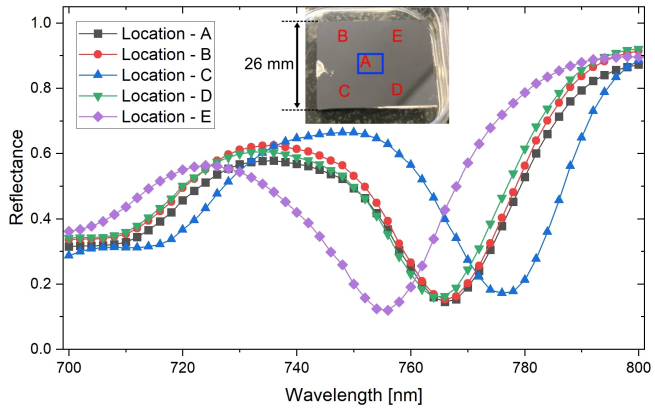

FIG. 6. Reflectance of the wafer at different locations measured in air after taking out the sample from the UHV chamber. Five different positions are represented by A, B, C, D, and E. Position C is close to the center, whereas position E is close to the edge of the wafer.

IV. CONCLUSION

In summary, this study involved the fabrication of superlattice GaAs/GaAsP photocathodes with a Distributed Bragg Reflector (DBR) structure using the molecular beam epitaxy technique. The resulting photocathodes exhibited favorable characteristics, as indicated by the photoluminescence and reflectance spectra observed at a wavelength of approximately 780 nm. Moreover, thorough transmission electron microscopy (TEM) analyses confirmed the presence of minimal crystal defects, while the superlattice (SL) and DBR structures were accurately identified. With this type of photocathodes, the achieved quantum efficiency exceeds 15%, surpassing the established benchmark. Additionally, electron spin polarization of up to 75% was attained when the photocathodes were illuminated with near bandgap photon energies. Notably, ongoing efforts are being dedicated to further optimization with the aim of attaining even higher quantum efficiencies and electron spin polarization levels.

SUPPLEMENTARY MATERIAL

See the supplementary material for QE and electron-spin polarization for the GaAs/GaAsP superlattice DBR photocathode as a function of the wavelength measured at the edge of the wafer.

ACKNOWLEDGMENTS

The work is supported by Brookhaven Science Associates, LLC under Contract DESC0012704 with the U.S. DOE. This research used resources of the Center for Functional Nanomaterials (CFN), which is a U.S. Department of Energy Office of Science User Facility, at BNL. This work was performed, in part, at the Center for Integrated Nanotechnologies, an Office of Science User Facility operated for the U.S. Department of Energy (DOE) Office of Science. This paper describes objective technical results and analysis. Any subjective views or opinions that might be expressed in the paper do not necessarily represent the views of the U.S. Department of Energy or the United States Government. This article has been authored by an employee of National Technology & Engineering Solutions of Sandia, LLC under Contract No. DE-NA0003525 with the U.S. Department of Energy (DOE). The employee owns all right, title and interest in and to the article and is solely responsible for its contents. The United States Government retains and the publisher, by accepting the article for publication, acknowledges that the United States Government retains a non-exclusive, paid-up, irrevocable, world-wide license to publish or reproduce the published form of this article or allow others to do so, for United States Government purposes. The DOE will provide public access to these results of federally sponsored research in accordance with the DOE Public Access Plan https://www.energy.gov/downloads/doe-public-access-plan.

AUTHOR DECLARATIONS

Conflict of Interest

The authors have no conflicts to disclose.

Author Contributions

Jyoti Biswas: Writing – original draft (lead); Writing – review & editing (equal); Investigation (equal); Formal analysis (equal); Conceptualization(equal). **Luca Cultrera:** Writing –

original draft (equal); Writing – review & editing (equal); Investigation (equal); Conceptualization (lead); Formal analysis (equal); Funding acquisition (lead). **Wei Liu:** Writing – review & editing (equal); Investigation (equal); Formal analysis (equal); Conceptualization(equal). **Erdong Wang:** Writing – review & editing (equal); Investigation (equal); Formal analysis (equal). **John Skaritka:** Writing – review & editing (supporting); Investigation (supporting). **Kim Kisslinger:** Writing – review & editing (supporting); Investigation (equal). **S.D. Hawkins:** Writing – review & editing (supporting); Investigation (supporting); **S.R. Lee:** Writing – review & editing (supporting); Investigation (supporting). **J.F. Klem:** Writing – review & editing (equal); Investigation (equal); Formal analysis (equal); Conceptualization(equal); Funding acquisition (equal);

DATA AVAILABILITY

The data that support the findings of this study are available from the corresponding author upon reasonable request.

REFERENCES

[1]M. Kuwahara, S. Kusunoki, X. G. Jin, T. Nakanishi, Y. Takeda, K. Saitoh, T. Ujihara, H. Asano, and N. Tanaka, Applied Physics Letters **101**, 033102 (2012).

[2]J. Dumas, J. Grames, and E. Voutier, AIP Conference Proceedings **1149**, 1184 (2009).

[3]C. Montag, E. Aschenauer, G. Bassi, J. Beebe-Wang, S. Benson, J. Berg, *et al.*, in *Proc. IPAC'21*, International Particle Accelerator Conference No. 12 (JACoW Publishing, Geneva, Switzerland, 2021) pp. 2585–2588.

[4]E. Wang, O. Rahman, J. Skaritka, W. Liu, J. Biswas, C. Degen, P. Inacker, R. Lambiase, and M. Paniccia, Phys. Rev. Accel. Beams **25**, 033401 (2022).

[5]P. Agostini, H. Aksakal, S. Alekhin, *et al.*, Journal of Physics G: Nuclear and Particle Physics **48**, 110501 (2021).

[6]Z. Liu, Y. Sun, S. Peterson, and P. Pianetta, Applied Physics Letters **92**, 241107 (2008).

[7]J. K. Bae, L. Cultrera, P. DiGiacomo, and I. Bazarov, Applied Physics Letters **112**, 154101 (2018).

[8]X. Jin, A. A. C. Cotta, G. Chen, A. T. N'Diaye, A. K. Schmid, and N. Yamamoto, Journal of Applied Physics **116**, 174509 (2014).

[9]J. K. Bae, A. Galdi, L. Cultrera, F. Ikponmwen, J. Maxson, and I. Bazarov, Journal of Applied Physics **127**, 124901 (2020).

[10]T. Nakanishi, H. Aoyagi, H. Horinaka, Y. Kamiya, T. Kato, S. Nakamura, T. Saka, and M. Tsubata, Physics Letters A **158**, 345 (1991).

[11]A. V. Subashiev, L. G. Gerchikov, Y. A. Mamaev, Y. P. Yashin, J. S. Roberts, D.-A. Luh, T. Maruyama, and J. E. Clendenin, Applied Physics Letters **86**, 171911 (2005).

[12]X. Jin, B. Ozdol, M. Yamamoto, A. Mano, N. Yamamoto, and Y. Takeda, Applied Physics Letters **105**, 203509 (2014).

[13]Y. A. Mamaev, L. G. Gerchikov, Y. P. Yashin, D. A. Vasiliev, V. V. Kuzmichev, V. M. Ustinov, A. E. Zhukov, V. S. Mikhrin, and A. P. Vasiliev, Applied Physics Letters **93**, 081114 (2008).

[14]X. Jin, A. Mano, F. Ichihashi, N. Yamamoto, and Y. Takeda, Applied Physics Express **6**, 015801 (2012).

[15]S. Zhang, S. Benson, and C. H-Garcia, Nuclear Instruments and Methods in Physics Research Section A: Accelerators, Spectrometers, Detectors and Associated Equipment **631**, 22 (2011).

[16]W. Liu, Y. Chen, W. Lu, A. Moy, M. Poelker, M. Stutzman, and S. Zhang, Applied Physics Letters **109**, 252104 (2016).

[17]L. G. Gerchikov, K. Aulenbacher, J. E. Clendenin, V. V. Kuz'michev, Y. A. Mamaev, T. Maruyama, V. S. Mikhrin, J. S. Roberts, V. M. Ustinov, D. A. Vasiliev, A. P. Vasiliev, Y. P. Yashin, and A. E. Zhukov, AIP Conference Proceedings **980**, 124 (2008).

[18]T. Saka, T. Kato, T. Nakanishi, M. Tsubata, *et al.*, Japanese Journal of Applied Physics **32**, L1837 (1993).

[19]J. C. Gröbli, D. Oberli, F. Meier, A. Dommann, Y. Mamaev, A. Subashiev, and Y. Yashin, Phys. Rev. Lett. **74**, 2106 (1995).

[20]T. Nishitani, O. Watanabe, T. Nakanishi, S. Okumi, K. Togawa, C. Suzuki, F. Furuta, K. Wada, M. Yamamoto, J. Watanabe, S. Kurahashi, M. Miyamoto, H. Kobayakawa, Y. Takeda, T. Saka, K. Kato, A. K. Bakarov, A. S. Jaroshevich, H. E. Scheibler, A. I. Toropov, and A. S. Terekhov, AIP Conference Proceedings **570**, 1021 (2001).

[21]G. D. Clark and N. Holonyak, Phys. Rev. **156**, 913 (1967).

[22]V. Emberger, F. Hatami, W. Ted Masselink, and S. Peters, Applied Physics Letters **103**, 031101 (2013).

[23]B. Monemar, Solid State Communications **8**, 2121 (1970).

[24]X. Jin, Y. Maeda, T. Sasaki, S. Arai, Y. Ishida, M. Kanda, S. Fuchi, T. Ujihara, T. Saka, and Y. Takeda, Journal of Applied Physics **108**, 094509 (2010).

[25]C. Y. Su, W. E. Spicer, and I. Lindau, Journal of Applied Physics **54**, 1413 (1983).

[26]"Svt associated, inc," .